J|A|C|S
ARTICLES
Published on Web 04/19/2005

Ultrafast Dynamics of ^2E State Formation in $Cr(acac)_3$

Eric A. Juban and James K. McCusker*

Contribution from the Department of Chemistry, Michigan State University, East Lansing, Michigan 48824

Received December 30, 2004; E-mail: jkm@cem.msu.edu

Abstract: Femtosecond time-resolved absorption spectroscopy has been used to elucidate the excited-state dynamics associated with formation of the ^2E excited state in a Cr^{III} transition metal complex. $Cr(acac)_3$ (where acac is the deprotonated monoanion of acetylacetone) exhibits monophasic decay kinetics with $\tau = 1.1 \pm 0.1$ ps following excitation into the lowest-energy ligand-field absorption band; the time constant is found to be independent of both excitation and probe wavelength across the entire $^4A_2 \rightarrow {}^4T_2$ absorption envelope. The lack of a significant shift in the excited-state absorption spectrum combined with the observed spectral narrowing is consistent with an assignment of this process as vibrational cooling (k_{vib}) in the ^2E state. The data on $Cr(acac)_3$ indicate that intersystem crossing associated with the $^4T_2 \rightarrow {}^2E$ conversion occurs at a rate $k_{ISC} > 10^{13}$ s^{-1} and furthermore competes effectively with vibrational relaxation in the initially formed $^4T_2$ state. Excitation into the higher energy ^{4}LMCT state ($\lambda_{ex} = 336$ nm) gives rise to biphasic kinetics with $\tau_1 = 50 \pm 20$ fs and $\tau_2 = 1.2 \pm 0.2$ ps. The slower component is again assigned to vibrational cooling in the ^2E state, whereas the subpicosecond process is attributed to conversion from the charge-transfer to the ligand-field manifold. In addition to detailing a process central to the photophysics of Cr^{III}, these results reinforce the notion that the conventional picture of excited-state dynamics in which $k_{vib} > k_{IC} > k_{ISC}$ does not generally apply when describing excited-state formation in transition metal complexes.

Introduction

The photochemical and photophysical properties of molecules constitute an important area of chemical research. In addition to providing insight into various aspects of electronic structure, photoinduced properties represent the basis upon which light-dependent molecular devices can be developed.[1−6] The rational design of such functional chromophores in turn depends greatly on a fundamental understanding of how molecules absorb and dissipate radiant energy. In the vast majority of cases, photoexcitation does not directly populate the lowest-lying electronic excited state of a molecule. Although the fully thermalized, lowest-energy excited state may persist for nanoseconds to microseconds—thereby allowing for bimolecular reactivity, for example—its formation generally occurs much more rapidly. Evolution from the Franck−Condon state to lower-energy excited states can involve a variety of processes. In particular, dynamics relating to internal conversion (IC), intersystem crossing (ISC), and vibrational relaxation (VR) are important factors in determining the dominant pathways of relaxation and, ultimately, the mechanism of excited-state evolution.

Ultrafast dynamics as they occur in transition metal complexes represent an active area of research at the interface of inorganic and physical chemistries.[7−9] Reports from a number of groups on a wide range of chemical systems continue to underscore the importance attached to these earliest stages of excited-state evolution. For example, electron and energy transfer processes have been identified that occur on subpicosecond time scales;[10−18] photochemical reactions including isomerization and ligand dissociation exhibiting rates in excess of 10^{12} s^{-1} have also been described.[19−26] In terms of applied

(1) Badjic, J. D.; Balzani, V.; Credi, A.; Silvi, S.; Stoddart, J. F. *Science* **2004**, *303*, 1845−1849.
(2) Hagfeldt, A.; Gratzel, M. *Acc. Chem Res.* **2000**, *33*, 269−277.
(3) Bignozzi, C. A.; Schoonover, J. R.; Scandola, F. *Prog. Inorg. Chem.* **1997**, *44*, 1−95.
(4) Colasson, B. X.; Dietrich-Buchecker, C.; Jimenez-Molero, M. C.; Sauvage, J. P. *Phys. Org. Chem.* **2002**, *15*, 476−483.
(5) Mobian, P.; Kern, J. M.; Sauvage, J. P. *Angew. Chem.* **2004**, *43*, 2392−2395.
(6) Venturi, M.; Balzani, V.; Ballardini, R.; Credi, A.; Gandolfi, M. T. *Int. J. Photoenergy* **2004**, *6*, 1−10.
(7) McCusker, J. K. *Acc. Chem Res.* **2003**, *36*, 876−887.
(8) Vlcek, A. *Coord. Chem. Rev.* **2000**, *200*, 933−977.
(9) For a more general discussion of the photophysical properties of transition metal complexes, see: Roundhill, D. M. *Photochemistry and Photophysics of Metal Complexes*; Plenum Press: New York, 1994.
(10) Fleming, C. N.; Maxwell, K. A.; DeSimone, J. M.; Meyer, T. J.; Papanikolas, J. M. *J. Am. Chem. Soc.* **2001**, *123*, 10336−10347.
(11) Son, D. H.; Kambhampati, P.; Kee, T. W.; Barbara, P. F. *J. Phys. Chem. A* **2002**, *106*, 4591−4597.
(12) Andersson, J.; Puntoriero, F.; Serroni, S.; Yartsev, A.; Pascher, T.; Polivka, T.; Campagna, S.; Sundstrom, V. *Faraday Discuss.* **2004**, *127*, 295−305.
(13) Torieda, H.; Nozaki, K.; Yoshimura, A.; Ohno, T. *J. Phys. Chem. A* **2004**, *108*, 4819−4829.
(14) Yoshimura, A.; Torieda, H.; Ohno, T. *J. Phys. Chem. A* **2004**, *108*, 2149−2154.
(15) Wang, C.; Mohney, B. K.; Akhremitchev, B. B.; Walker, G. C. *J. Phys. Chem. A* **2000**, *104*, 4314−4320.
(16) Shaw, G. B.; Styers-Barnett, D. J.; Gannon, E. Z.; Granger, J. C.; Papanikolas, J. M. *J. Phys. Chem. A* **2004**, *108*, 4998−5006.
(17) Polivka, T.; Pullerits, T.; Frank, H. A.; Cogdell, R. J.; Sundstrom, V. *J. Phys. Chem. B* **2004**, *108*, 15398−15407.
(18) Kambhampati, P.; Son, D. H.; Kee, T. W.; Barbara, P. F. *J. Phys. Chem. A* **2000**, *104*, 10637−10644.
(19) Farrell, I. R.; Matousek, P.; Towrie, M.; Parker, A. W.; Grills, D. C.; George, M. W.; Vlcek, A. *Inorg. Chem.* **2002**, *41*, 4318−4323.
(20) Farrell, I. R.; Matousek, P.; Vlcek, A. *J. Am. Chem. Soc.* **1999**, *121*, 5296−5301.

research, the use of transition metal complexes as sensitizers for wide-band gap semiconductors is dependent on charge injection from the chromophore into the conduction band of the semiconductor.[2] The efficiency of this process reflects a competition between the rate of interfacial electron transfer and intramolecular dynamics that serve to relax the excited state of the sensitizer.[27,28] It has been suggested that "hot" injection—electron transfer prior to excited-state thermalization—is an important mechanism to exploit for the development of more efficient devices based on this technology.[29] In all of these settings, detailed studies of the processes that ensue immediately following photon absorption are critically important.

The specifics of nonradiative decay are primarily governed by the relative rates of electronic surface crossings and vibrational relaxation processes available to a given excited state. Conventional models of these events are derived largely from observations on organic molecules.[30] These systems, with their relatively low number of electronic states and relatively high vibrational frequencies, tend to be characterized by a relaxation cascade in which vibrational relaxation occurs first, followed by internal conversion, and last, intersystem crossing (i.e., $k_{VR} > k_{IC} > k_{ISC}$). This model, though conceptually appealing, is finding limited applicability for describing excited-state evolution in metal-containing systems. Intersystem crossing in $[Ru(bpy)_3]^{2+}$, for example, occurs with a time constant of $\tau = 40 \pm 15$ fs,[31] whereas vibrational cooling in the ^{3}MLCT state takes place on the order of several picoseconds.[32] Our group has documented the case of a low-spin Fe^{II} complex that undergoes conversion to its excited $^5T_2$ ligand-field state following $^1A_1 \rightarrow {}^1$MLCT excitation in ~500 fs: this is a net $\Delta S = 2$ transition with a rate exceeding 10^{12} s^{-1}.[33] These are two of many examples that demonstrate the need for a comprehensive reassessment of the present picture of inorganic photophysics as it pertains to the mechanism by which the excited states of transition metal complexes are formed.

Our research efforts over the past several years have focused on the use of femtosecond absorption spectroscopy to begin redressing the issue of excited-state evolution in inorganic compounds; in this report we turn our attention to the dynamics of Cr^{III}. With the possible exception of Ru^{II}, the excited-state properties of Cr^{III} are the most thoroughly studied of any transition metal ion and, consequently, help form the underpinning of the fields of inorganic photophysics and photochemistry.[34−36] The vast amount of previous research on Cr^{III} in terms of the range of complexes available as well as prior time-resolved spectroscopic studies provides an excellent starting point for ultrafast work. Additionally, we are interested in dynamics following both ligand-field and charge-transfer excitation. In the case of the former, there is virtually nothing known for any transition metal-containing system. Any number of Cr^{III} complexes have ground-state absorptive properties that allow access to both types of excited-state manifolds.

The lowest-lying excited state for most Cr^{III} complexes is a ^{2}E, which corresponds to an intraconfigurational excited state of the $^4A_2$ ground state. The photophysical properties of Cr^{III} complexes are inexorably tied to this excited state. The ^{2}E state possesses a relatively long lifetime (e.g., nanosecond to microsecond) and is weakly emissive in rigid media and/or at low temperature. However, the absorption cross section is exceedingly small ($\epsilon \approx 1$ M^{-1} cm^{-1}), consistent with its spin-forbidden character. Population of the ^{2}E therefore occurs via nonradiative decay from higher-lying states. The ^{2}E state itself and its subsequent decay back to the ground state have been characterized in detail for a large number of complexes.[35−37] However, the details of the formation of this state following photoexcitation into one of the spin-allowed absorptions remain largely obscure. The most definitive work to date on this subject is that of Rojas and Magde, who reported an instrument-limited absorptive feature (1−2 ps) that was attributed to formation of the ^{2}E state in $Cr(acac)_3$ following charge-transfer excitation at 314 nm.[38]

Given this previous report, we selected $Cr(acac)_3$ as a prototype for the study of the ultrafast spectroscopy of Cr^{III} complexes.[39−43] In addition to providing a more accurate assessment of the formation time of the ^{2}E state for this compound, analysis of the femtosecond differential absorption spectra has provided insights into a variety of relaxation dynamics that occur after photoexcitation. The result is a reasonably complete picture of the mechanism of excited-state evolution in a system that we believe can serve as a model for the ultrafast excited-state dynamics of simple Cr^{III} coordination compounds.

Experimental Section

Materials. $Cr(acac)_3$ was purchased from Aldrich and recrystallized twice from methanol. Spectral-grade acetonitrile was used as received from Aldrich. For the low-temperature spectroscopy, a mixture of propionitrile and butyronitrile (9:2) readily formed an optical glass after being dried over calcium hydride.

Static and Nanosecond Time-Resolved Spectroscopies. Static absorption, emission, and nanosecond time-resolved absorption measurements were carried out as previously described.[44] Low-temperature

(21) Fuss, W.; Trushin, S. A.; Schmid, W. E. *Res. Chem. Intermed.* **2001**, *27*, 447−457.
(22) Lian, T.; Bromberg, S. E.; Asplund, M.; Yang, H.; Harris, C. B. *J. Phys. Chem.* **1996**, *100*, 11994−12001.
(23) Lee, M.; Harris, C. B. *J. Am. Chem. Soc.* **1989**, *111*, 8963−8965.
(24) Zalis, S.; Busby, M.; Kotrba, T.; Matousek, P.; Towrie, M.; Vlcek, A. *Inorg. Chem.* **2004**, *43*, 1723−1734.
(25) Vlcek, A.; Farrell, I. R.; Liard, D. J.; Matousek, P.; Towrie, M.; Parker, A. W.; Grills, D. C.; George, M. W. *J. Chem. Soc., Dalton Trans.* **2002**, 701−712.
(26) Vlcek, A. *Coord. Chem. Rev.* **2002**, *230*, 225−242.
(27) Benko, G.; Kallioinen, J.; Myllyperkio, P.; Trif, F.; Korppi-Tommola, J. E. I.; Yartsev, A. P.; Sundstrom, V. *J. Phys. Chem. B* **2004**, *108*, 2862−2867.
(28) Anderson, N. A.; Ai, X.; Lian, T. *J. Phys. Chem. B* **2003**, *107*, 14414−14421.
(29) Nozik, A. J. *Annu. Rev. Phys. Chem.* **2001**, *52*, 193−231.
(30) Turro, N. J. *Modern Molecular Photochemistry*; University Science Books: Mill Valley, CA, 1991.
(31) Bhasikuttan, A. C.; Suzuki, M.; Nakashima, S.; Okada, T. *J. Am. Chem. Soc.* **2002**, *124*, 8398−8405.
(32) Damrauer, N. H.; McCusker, J. K. *J. Phys. Chem. A* **1999**, *103*, 8440−8446.
(33) Monat, J. E.; McCusker, J. K. *J. Am. Chem. Soc.* **2000**, *122*, 4092−4097.
(34) Forster, L. S. *Chem. Rev.* **1990**, *90*, 331−353.
(35) Kirk, A. D. *Chem. Rev.* **1999**, *99*, 1607−1640.
(36) Endicott, J. F.; Ramasami, T.; Tamilarasan, R.; Lessard, R. B.; Ryu, C. K.; Brubaker, G. R. *Coord. Chem. Rev.* **1987**, *77*, 1−87.
(37) Forster, L. S. *Coord. Chem. Rev.* **2002**, *227*, 59−92.
(38) Rojas, G. E.; Dupuy, C.; Sexton, D. A.; Magde, D. *J. Phys. Chem.* **1986**, *90*, 87−92.
(39) The work described herein concerns ultrafast photophysics. Other workers have explored the ultrafast photochemistry of Cr^{III} complexes in various contexts (cf. 19, 20, 22, 23).
(40) Shaw, L. E.; Langford, C. H. *Inorg. Chem.* **2000**, *39*, 541−546.
(41) Wang, L.; Zhu, X.; Spears, K. G. *J. Am. Chem. Soc.* **1988**, *110*, 8695−8696.
(42) Lesage, R.; Sala, K. L.; Yip, R. W. *Can. J. Chem.-Rev. Can. Chim.* **1983**, *61*, 2761−2766.
(43) Serpone, N.; Hoffman, M. Z. *J. Phys. Chem.* **1987**, *91*, 1737−1743.
(44) Damrauer, N. H.; Boussie, T. R.; Devenny, M.; McCusker, J. K. *J. Am. Chem. Soc.* **1997**, *119*, 8253−8268.

data were acquired using a Janis SVT-100 optical dewar according to protocols discussed elsewhere.[45]

Femtosecond Transient Absorption Spectroscopy. Ultrafast measurements were carried out as described elsewhere,[32] with the following modifications: The Ti:sapphire oscillator (Coherent Mira 900), formerly coupled to an Ar-ion laser, is now pumped by a diode-pumped Nd:YVO_4 laser (Coherent Verdi) operating at 5.40 W. Excitation wavelengths throughout the visible and near-UV were afforded by a Quantronix TOPAS optical parametric amplifier coupled to a Positive Light Spitfire Ti:sapphire regenerative amplifier operating at 805 nm (1 W, 85 fs). Cross-correlation pulse widths at the sample yielded values in the range of 90−100 fs. In addition to the previously described single-wavelength detection scheme, the CCD has now been replaced with a Hamamatsu NMOS photodiode array to collect full spectra. The diode array yielded a greater than 5-fold increase in signal-to-noise ratio for the full spectrum data relative to the CCD under similar conditions, primarily due to the higher saturation threshold of the diode array. The white light probe beam was generated by self-phase modulation in either sapphire or calcium fluoride using residual output from the regen. The CaF_2 setup employed a disk 6 mm in thickness mounted on a continuously moving linear slide.

Typical pump powers were 6−7 μJ for visible excitation and 1−2 μJ for 335-nm excitation. Sample ground-state absorbances were approximately 0.5 at the excitation wavelength in a 1-mm path-length cell. All kinetics were checked for linearity with respect to pump power as well as concentration of the chromophore over a range of roughly 1 order of magnitude. Particularly under visible excitation, solvent blanks showed large nonlinear signals when the pump and probe beams were simultaneously present in the sample.[46] We were unable to quantitatively account for these signals in the kinetic models; fits of data were therefore begun at times after the solvent signal had disappeared. To confirm the presence of the early-time component under 335-nm excitation, additional measurements were taken in 0.2-mm path-length cells, which gave solvent signals of lower intensity and shorter duration. Monoexponential fits to the data were carried out using the Origin software package. For the biexponential data, which contained a kinetic component comparable in time scale to the excitation pulse, an instrument response function was collected using 2-methylnaphthalene as a two-photon absorber. This response function was fit to a Gaussian, which was then iteratively reconvolved with the kinetic model using a program of local origin.

Chirp-Corrected, Time-Dependent Full Spectra. The chirp in our probe beam is approximately 200 fs over a spectral window of 470−700 nm. To correct for this distortion of the spectra at early times (Δt < 1 ps), solvent-only spectra were recorded immediately prior to data acquisition on the chromophore.[47] Groups of ~30 pixels (corresponding to a bandwidth of ~10 nm) were averaged together, and $\Delta t = 0$ was then determined by direct examination of this average as a function of translation stage position. This process was repeated at intervals of 30 nm across the entire photodiode array. Although spectral chirp does not in general follow a linear dependence, the variation in $\Delta t = 0$ with wavelength was well-approximated by a linear regression over the ~200-nm window available with our spectrometer. A temporal correction factor for each pixel was generated with this regression and applied to the data as described below.

Transient absorption data on Cr(acac)$_3$ were collected at stage positions corresponding to 20-fs increments. Pixels of the diode array were therefore grouped together in 20-fs blocks according to the correction factors obtained from the solvent-only data. For example, at stage position A pixels 50−67 were assigned to $\Delta t = 300$ fs, pixels 68−85 to $\Delta t = 280$ fs, and pixels 86−103 to $\Delta t = 260$ fs. Stage position B, 20 fs later, corresponded to $\Delta t = 320$ for pixels 50−67, $\Delta t = 300$ fs for pixels 68−85, and so on. The $\Delta t = 300$ fs data for each block of pixels were combined and reported together as the complete $\Delta t = 300$ fs spectrum. This process was repeated every 20 fs, yielding the complete differential spectra as a function of time. This method works quite well provided the spectrum does not change appreciably between adjacent stage positions. If this condition is not met, discontinuities in the spectral profile are obtained at the boundaries of each pixel block. However, this problem may be alleviated by increasing the density of collected stage positions to yield increments in Δt for which $\Delta\Delta A$ approaches zero.

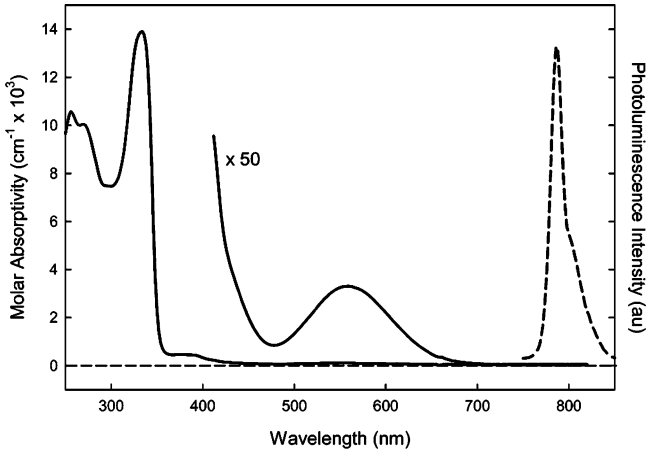

Figure 1. Ground-state absorption (solid line) and low-temperature emission (dashed line) spectra of Cr(acac)$_3$. The lowest-energy absorption feature is assigned to the $^4A_2 \rightarrow {}^4T_2$ transition, whereas emission arises from the intraconfigurational ^2E state.

Results and Discussion

Electronic Structure of Cr(acac)$_3$. For our initial studies on the ultrafast dynamics of Cr^{III}, we desired a molecule with a relatively simple electronic structure, a high degree of photostability, and the opportunity for excitation into both ligand-field and charge-transfer states. Cr(acac)$_3$ meets all of these criteria: it is essentially octahedral, its quantum yield for photosubstitution has been reported as 0.01,[48] and its photophysical properties on longer time scales (i.e., the spectroscopy of its lowest-energy excited state) have been thoroughly documented.[49−53]

The absorption and low-temperature emission spectra of the complex are shown in Figure 1. The ground state is $^4A_2$,[54] represented in a one-electron orbital approximation as shown in the following illustration:

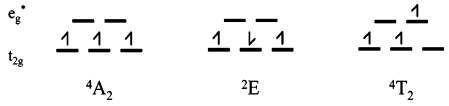

The lowest-energy excited state is a ^2E state corresponding to an intraconfigurational spin flip. The $^2E \rightarrow {}^4A_2$ transition is

(45) Damrauer, N. H.; McCusker, J. K. *Inorg. Chem.* **1999**, *38*, 4268−4277.
(46) Kovalenko, S. A.; Dobryakov, A. L.; Ruthmann, J.; Ernsting, N. P. *Phys. Rev. A* **1999**, *59*, 2369−2384.
(47) Under visible excitation, large nonlinear signals arose when both pump and probe beams were present in the sample. $\Delta t = 0$ could be determined from these alone. For wavelength regions where the solvent-only signal is smaller, an appropriate two-photon absorber was used.
(48) Zinato, E.; Riccieri, P.; Sheridan, P. S. *Inorg. Chem.* **1979**, *18*, 720−724.
(49) Krause, R. A.; Trabjerg, I.; Ballhausen, C. J. *Acta Chem. Scand.* **1970**, *24*, 593−597.
(50) Atanasov, M. A.; Schonherr, T. *Inorg. Chem.* **1990**, *29*, 4545−4550.
(51) Chen, S.; Porter, G. B. *J. Am. Chem. Soc.* **1970**, *92*, 2189−2190.
(52) Ohno, T.; Kato, S. *Bull. Chem. Soc. Jpn.* **1970**, *43*, 8−12.
(53) Yardley, J. T.; Beattie, J. K. *J. Am. Chem. Soc.* **1972**, *94*, 8925−8926.
(54) Although the molecular symmetry is more accurately D_3, the trigonal splittings in this molecule are on the order of 100 cm^{-1} (cf. 50). Throughout this report we will retain octahedral symmetry labels.

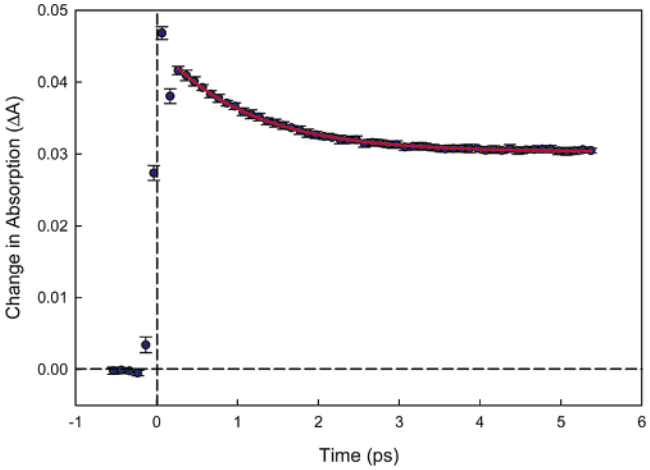

Figure 2. Time-resolved absorption data for $Cr(acac)_3$ at 480 nm, following ~100-fs excitation of a room-temperature CH_3CN solution at 625 nm. The solid line corresponds to a monoexponential fit with a time constant of 1.09 ± 0.06 ps.

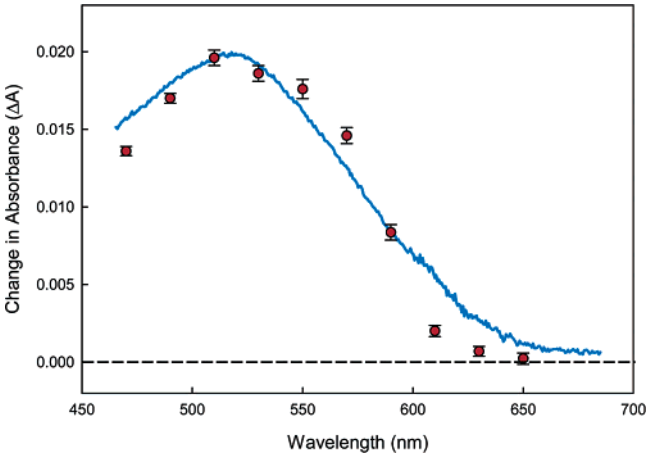

Figure 3. Transient absorption spectrum of $Cr(acac)_3$ in CH_3CN solution at $\Delta t = 5$ ps, along with normalized absorption amplitudes obtained from single-wavelength nanosecond transient absorption data obtained in a 9:2 propionitrile/butyronitrile glass at 90 K. The agreement between the two data sets confirms that $Cr(acac)_3$ is in its fully thermalized, lowest electronic excited state (^2E) by the time the dynamics illustrated in Figure 2 are complete.

responsible for the static emission spectrum centered at 794 nm. The band is narrow, as expected for a radiative transition between two states with minimal nuclear equilibrium displacement (i.e., nested potential energy surfaces). The corresponding absorption does not appear due to its exceedingly low oscillator strength.

The lowest-energy absorption in room-temperature solution, with a maximum at 560 nm, corresponds to the $^4A_2 \rightarrow {}^4T_2$ ligand-field transition. Excitation into the $^4T_2$ state involves a change in orbital population, where one electron from the nonbonding t_{2g} orbitals now resides in an antibonding e_g* orbital. Because of the antibonding nature of the e_g* orbitals, there is a large displacement in nuclear equilibrium relative to the ground state of the molecule, resulting in a relatively broad absorption band. This proves to be very useful for our variable excitation wavelength experiments: tuning the pump wavelength across the entire band allows the amount of excess vibrational energy in the excited state to be varied by more than 4000 cm^{-1} without changing the identity of the electronic states involved.

Below 400 nm, the absorption spectrum reveals the onset of the charge-transfer manifold. As expected, these transitions have much larger oscillator strengths. In addition to affording facile direct charge-transfer excitation from the ground state, the presence of these states assists in probing dynamics within the ligand-field manifold as well. Transient absorption studies of ligand-field states suffer from their inherently low absorption coefficients. This can be counteracted to some extent by increasing sample concentration, but the problem becomes amplified if the excited-state absorptions are also ligand-field in nature. In the case of $Cr(acac)_3$, the charge-transfer states accessible with ultraviolet photons from the ground state give rise to visible absorptions from the low-lying ligand-field excited states (e.g., the ^2E and $^4T_2$ terms). This allows us to exploit charge-transfer-type oscillator strengths for probing dynamics in the ligand-field manifold, resulting in a significantly higher signal-to-noise ratio for the transient absorption measurements.

Ligand-Field Excitation. At all pump and probe wavelengths monitored, excited-state dynamics following excitation into the $^4A_2 \rightarrow {}^4T_2$ absorption were complete within several picoseconds. Representative ultrafast transient absorption data are shown in Figure 2, where excitation at 625 nm yields an instrument-limited initial absorption that decays monoexponentially with a time constant of 1.09 ± 0.06 ps.[55] No additional dynamics are observed until the onset of ground-state recovery, which we estimate to have a time constant of ~700 ps. A full spectrum at $\Delta t = 5$ ps is shown in Figure 3, along with nanosecond transient absorption data acquired at 90 K. The agreement supports our assignment that the long-lived feature corresponding to the baseline offset in the ultrafast data is due to absorption of the fully thermalized ^2E excited state.

To further explore the early time dynamics, we employed pump wavelengths from 505 to 645 nm and probe wavelengths from 450 to 780 nm. Figure 4 displays chirp-corrected time-dependent full spectra along with three relevant single-wavelength kinetics traces following excitation on the low-energy shoulder of the $^4T_2$ absorption (625 nm). Although in principle the entirety of the dynamics may be represented with the time-dependent full spectra, utilizing data obtained from both methods of detection has proved invaluable to our analysis. Without the photodiode array we would be forced to reconstruct spectra from absorption amplitudes from our single-wavelength data. Changes in pump/probe overlap, fluctuations in pump power, and other factors as separate scans are taken at each probe wavelength can lead to difficulties establishing accurate relative values of ΔA across an entire absorption spectrum. On the other hand, the single-wavelength data exhibit much higher signal-to-noise, primarily due to the use of the lockin amplifier. The increased precision enables us to more readily compare time constants as a function of pump and probe wavelength, as well as to detect changes in ΔA as low as 10^{-5}. By using data from both detection schemes, we obtained a more accurate overall picture of the spectral evolution.

Both the single-wavelength and full-spectrum data reveal that the excited-state absorption spectrum of $Cr(acac)_3$ narrows, concomitant with a slight red shift, on a ~1-ps time scale. The single-wavelength traces show monoexponential absorptive decay at probe wavelengths from 450 to 550 nm, no kinetics

(55) Data were fit to an equation of the form $y(t) = c_1 \exp(-t/\tau) + a_0$, where a_0 corresponds to the offset at long delay times.

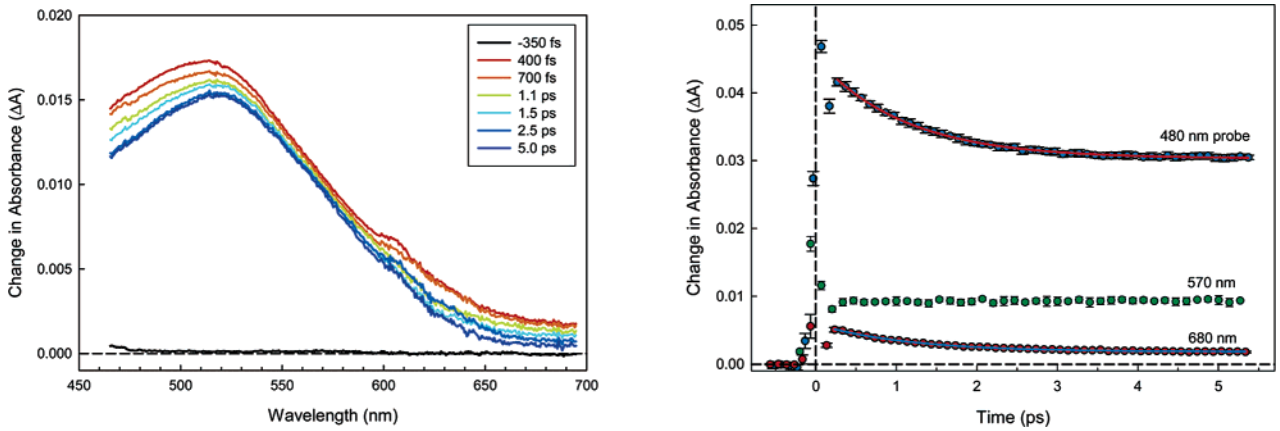

Figure 4. Time-resolved absorption data for $Cr(acac)_3$ in CH_3CN solution following ~100-fs excitation at 625 nm. (Left) Chirp-corrected, time-dependent full spectra. Noise in the data between 610 and 640 nm is due to scatter from the pump beam. The legend indicates delay times relative to the excitation pulse. (Right) Single-wavelength kinetics traces at 480, 570, and 680 nm. The solid lines correspond to fits of the data. See text for further details.

following the instrument-limited initial absorption at 560−570 nm, and the reemergence of monoexponential absorptive decay at wavelengths longer than 570 nm. There is no variation in the observed time constant at all pump and probe wavelengths monitored, as demonstrated by the data shown in Figure 5.

In this simple system, the only relaxation channels available following ligand-field excitation are vibrational relaxation within the $^4T_2$ state, intersystem crossing from the $^4T_2$ to the ^2E, and vibrational relaxation within the ^2E state. The relative rates of these processes are not known a priori. An assignment of the ~1-ps process to one or the other, or a combination of any or all, must therefore be made cautiously.

Intersystem Crossing versus Vibrational Relaxation. In the context of electronic transient absorption spectroscopy, differentiating between processes occurring on a single excited-state potential surface (e.g., vibrational relaxation) and surface-crossing dynamics associated with a change in electronic structure (e.g., intersystem crossing) can only be done definitively with prior knowledge of the absorption profiles of the different excited states involved. For transition metal compounds, the complexity of their electronic structures makes this an exceedingly difficult task. Techniques such as spectroelectrochemistry have proven useful in guiding assignments associated with charge-transfer states.[33,44] Various computational methods have also shown considerable promise in this regard.[56,57] When dealing with states other than the lowest-energy excited state of the system, however, one must generally rely on chemical intuition as to whether two different electronic states will exhibit distinct absorptive profiles. For example, significant differences can reasonably be expected for surface crossings corresponding to interconfigurational transitions; intraconfigurational dynamics might exhibit changes that are more subtle. The influence of solvation or other mechanisms of excited-state decay (e.g., vibrational relaxation) may also serve as complicating factors in the interpretation of transient absorption data. In previous studies of $[Ru(bpy)_3]^{2+}$,[58,59] for example, we identified a time constant for the formation of the lowest-lying excited state—in this case a ^{3}MLCT—of ~100 fs. This estimate was based on the evolution of time-dependent full spectra, which essentially stopped shifting by $\Delta t = 300$ fs. In that report, we were careful not to ascribe this to intersystem crossing, since a number of excited-state processes could in principle give rise to such shifts. To more accurately extract the actual rate of intersystem crossing, Okada and co-workers employed ultrafast fluorescence upconversion spectroscopy.[31] This technique is based on radiative coupling between the ground and excited states being sampled and is therefore inherently better suited to monitor a process associated with a change in spin (e.g., intersystem crossing); the value of 40 ± 15 fs that they report clearly demonstrates that the interpretation of dynamics from transient absorption spectra must be done carefully.

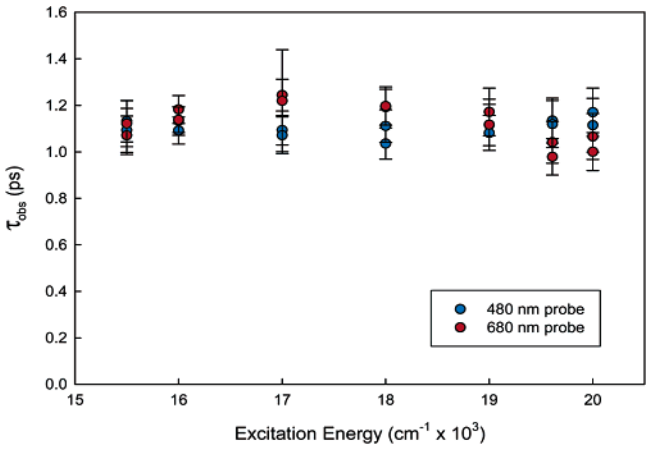

Figure 5. Time constant associated with the formation of the fully thermalized ^2E excited state as a function of pump energy at two representative probe wavelengths. The values obtained are within experimental error at all pump and probe wavelengths examined.

To understand the types of signals we might anticipate due to vibrational relaxation, we will make use of the potential energy surface diagram shown in Figure 6. This represents a generic three-state system consisting of a ground state and two electronic excited states, including vibrational sublevels along a single vibrational mode. Modeling the transient absorption experiment, pump photons create an excited-state population

(56) Daniel, C. *Coord. Chem. Rev.* **2003**, *238*, 143−166.
(57) Monat, J. E.; Rodriguez, J. H.; McCusker, J. K. *J. Phys. Chem. A* **2002**, *106*, 7399−7406.
(58) Damrauer, N. H.; Cerullo, G.; Yeh, A.; Boussie, T. R.; Shank, C. V.; McCusker, J. K. *Science* **1997**, *275*, 54−57.
(59) Yeh, A. T.; Shank, C. V.; McCusker, J. K. *Science* **2000**, *289*, 935−938.

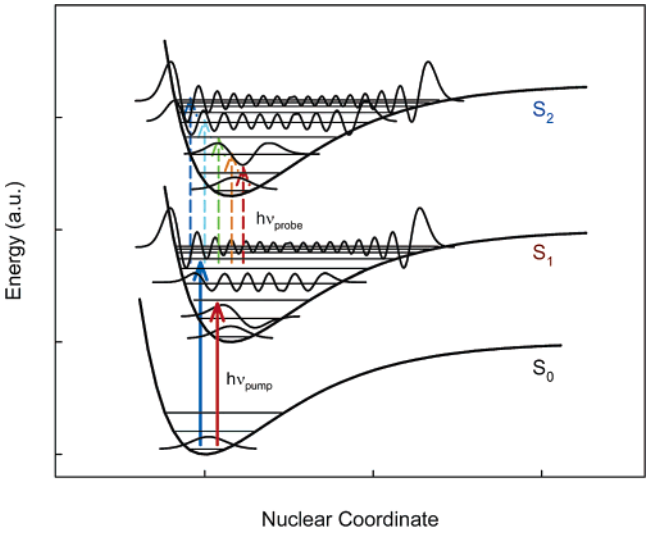

Figure 6. Generalized potential energy surface diagram for a three-state system. Pump photons ($h\nu_{pump}$) create an excited-state population in S_1, and probe photons ($h\nu_{probe}$) monitor absorptive transitions between S_1 and S_2. The latter are governed by Franck−Condon factors determined by the overlap of the vibrational wave functions in S_1 and S_2.

in S_1, while probe photons monitor the absorption between S_1 and S_2. The vibrational relaxation dynamics occur on the S_1 surface; the transient absorption signals are determined by the Franck−Condon factors between vibrational levels of S_1 and S_2.

Time constants assigned to vibrational relaxation processes can depend on both pump and probe wavelengths. Variation of the pump wavelength corresponds to placing the excited state at different depths of the S_1 potential well. At the top of the well, increased anharmonicity and the resulting higher density of states can facilitate vibrational relaxation. In accord with this, relaxation rates have indeed been shown to systematically increase with excitation energy in a number of organic systems.[60,61]

Variations in the observed kinetics with changes in probe wavelength can be described in a similar context. It is important to emphasize that, in contrast to changes in pump wavelength, the actual vibrational cooling rate (i.e., the time dependence of the change in population of vibrational levels of the S_1 surface) cannot depend on probe wavelength: the probe beam samples but does not influence the molecular dynamics. An experimentally observed dependence of kinetics on probe wavelength is a consequence of changes in the absorption cross section of the molecule as the system vibrationally cools. Generally speaking, higher-lying vibrational states on the S_1 surface have a wider range of transitions available than lower-lying ones. This may be rationalized by considering differences in the Franck−Condon factors at the top versus the bottom of the S_1 and S_2 potential energy surfaces. As vibrational cooling on the S_1 surface occurs, the Franck−Condon factors become more centralized around the equilibrium nuclear displacement. Two effects on the observed dynamics may result: (1) the absorption spectrum narrows as vibrational relaxation takes place[61,62] and (2) the observed time constant can vary with probe wavelength.[23,63] For example, one can envision a very low energy probe photon that shows absorption at the top of the S_1 potential well, but falls out of resonance with the $S_1 \rightarrow S_2$ transition at the bottom. A single-wavelength kinetics trace at this wavelength would show a faster time constant compared to a (shorter) wavelength that absorbs at both the top and bottom of the S_1 surface, even though both probe wavelengths are sampling the same physical process with the same intrinsic kinetics.

Turning now to the specific molecule in question, Figure 7 displays the potential energy surfaces relevant to the excited-state dynamics of $Cr(acac)_3$. The ^2E state assumes the role of the S_1 state in Figure 6. Although the ^2E state is not excited directly in the present case, whether the excited-state population of the lower-energy excited state is created optically or nonradiatively does not affect the analysis of its subsequent dynamics. Although the shapes of these potential surfaces are qualitative (i.e., derived from a generic Lennard-Jones potential), their relative positions are based in part on experimental data. For example, the minimum of the ^2E state can be estimated from the energy of the $0 \rightarrow 0$ transition observed in the compound's emission spectrum (Figure 1). The displacement of the $^4T_2$ surface is based on its absorption maximum (Figure 1) coupled with an estimate of the Huang−Rhys factor for a $(t_{2g})^2(e_g^*)^1$ configuration.[64] Finally, the charge-transfer states reflect the energies of the ground-state (^{4}LMCT) and excited-state (^{2}LMCT) absorption spectra.

The most striking aspect of the time-resolved full spectra in Figure 4 is the lack of any significant spectral shift or change in overall spectral profile associated with the ~1-ps decay process. To interpret these observations, we need to consider what changes in absorption spectrum, if any, we might expect to accompany the $^4T_2 \rightarrow {}^2E$ conversion. While the data in Figure 3 provide us with the absorption spectrum of the ^2E state, we

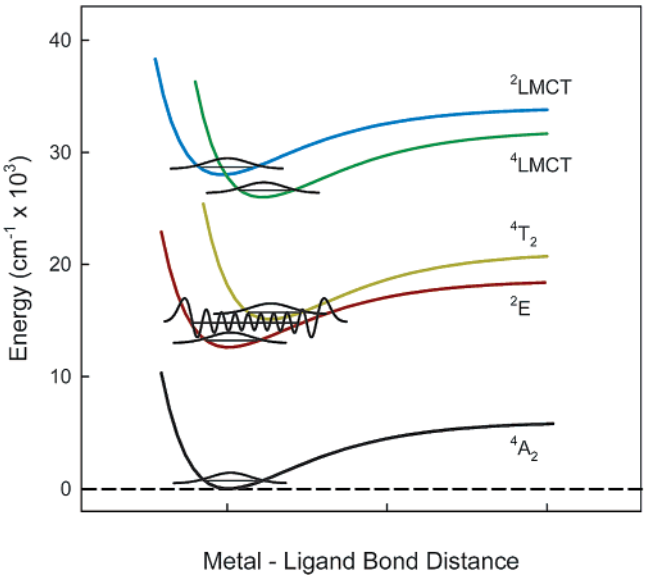

Figure 7. Semiquantitative potential energy surface diagram for $Cr(acac)_3$. The energy of the ground state was arbitrarily set to $E = 0$; the energies and displacements of the excited states were estimated from experimental data. See text for further details.

(60) Martini, I.; Hartland, G. V. *J. Phys. Chem. A* **1996**, *100*, 19764−19770.
(61) Kliner, D. A. V.; Alfano, J. C.; Barbara, P. F. *J. Chem. Phys.* **1993**, *98*, 5375−5389.
(62) Kuhne, T.; Kuster, R.; Vohringer, P. *Chem. Phys.* **1998**, *233*, 161−178.
(63) An estimate of 0.3 eV for the $^4T_2/^4A_2$ reorganization energy was taken as half the value found for the $^5T_2 \rightarrow {}^1A_1$ conversion in Fe^{II} (McCusker, J. K. Ph.D. Thesis, University of Illinois, 1992).
(64) Bingemann, D.; King, A. M.; Crim, F. F. *J. Chem. Phys.* **2000**, *113*, 5018−5025.

do not have any direct information concerning the spectrum of the $^4T_2$. We can, however, speculate on differences between the two states that might be anticipated. The π-donor characteristics of acac$^-$ make an LMCT-type transition to the t_{2g} orbitals of Cr^{III} the most likely origin of excited-state absorption for both the $^4T_2$ and ^2E states. The following illustration gives a one-electron representation of these LMCT states:

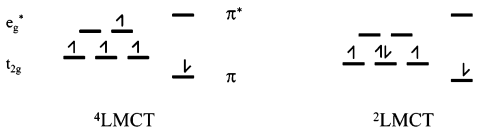

On the basis of the diagram shown, the potential energy surfaces corresponding to the ^{4}LMCT and ^{2}LMCT configurations are likely to have similar displacements relative to the $^4T_2$ and ^2E, respectively. This will translate into absorption bands of roughly similar breadth for transitions arising out of these two ligand-field excited states. However, the energies of these absorptions (i.e., λ_{max}) should be significantly different. An LMCT for the $^4T_2$ state can couple to an empty t_{2g} orbital, whereas the corresponding transition for the ^2E state will result in a $(t_{2g})^4$ configuration, requiring double occupancy of one of these orbitals. The resulting higher energy of the ^{2}LMCT state compared to that of the ^{4}LMCT, combined with the lower energy of the ^2E compared to that of the $^4T_2$, leads us to anticipate a significantly higher energy for the $^2E \rightarrow {}^2$LMCT transition. We recognize that this is a simplistic representation: the observed absorption features for coordination compounds derive from transitions between multielectronic states and are not quantitatively described by the one-electron picture just discussed. Nevertheless, we consider it *highly unlikely* that the $^4T_2$ and ^2E states would exhibit essentially identical absorption spectra, as the data in Figure 4 would require if the observed kinetics were monitoring the $^4T_2 \rightarrow {}^2E$ conversion.

On the basis of this conclusion, vibrational cooling would appear to be the only process assignable to the ~1-ps decay shown in Figure 3. Our data, however, do not reveal any dependence of the observed time constant on either pump or probe wavelength. These observations are not wholly consistent with the previously discussed model of vibrational relaxation. There are important differences, however, between Cr(acac)$_3$ and the organic molecules that make up the majority of the ultrafast literature where such effects have been documented. Pump wavelength-dependent variation of the vibrational relaxation rate depends on the potential energy landscape (e.g., density of states) being different at the top versus the bottom of an electronic potential well. Increasing the number of modes, particularly low-frequency modes with small energy spacings that are characteristic of coordination compounds, attenuates this difference. When this difference is sufficiently small, a pump wavelength dependence may no longer be experimentally observed.

Although we observe no variation in time constant as a function of probe wavelength, we do see a time-dependent narrowing of the excited-state absorption spectra. The preceding discussion concerning the effect of density of states notwithstanding, it is reasonable to expect that higher-lying vibrational levels will still show a wider range of absorptions than lower-lying ones due to the increased breadth of the potential at higher energies. We believe this is the origin of the observed narrowing

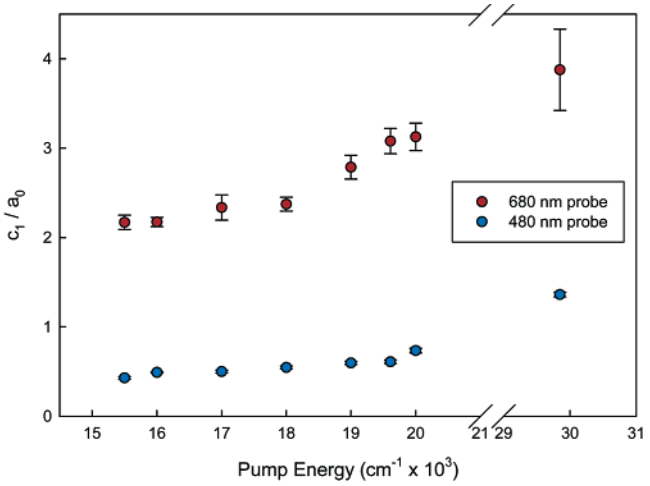

Figure 8. Comparison of the initial absorption amplitudes from single-wavelength kinetics traces as a function of excitation energy for two probe wavelengths. The constants c_1 and a_0 are values of the pre-exponential amplitude and long-time offset, respectively, from individual mono-exponential fits at each wavelength combination. The larger values of c_1/a_0 with increasing excitation energy indicate that the transient spectra are broader with higher-energy excitation.

of the transient spectrum. Dependence of τ_{obs} on probe wavelength should be attenuated in coordination complexes based on arguments analogous to those discussed above for τ_{pump}. We believe such variations in our molecule, if present, are within the experimental error of our measurements. We therefore assign the ~1-ps process shown in Figure 3 to vibrational relaxation in the ^2E state of Cr(acac)$_3$. Intersystem crossing associated with the $^4T_2 \rightarrow {}^2E$ conversion must therefore be faster than our time resolution (i.e., $k_{ISC} > 10^{13}$ s^{-1}).

With this assignment in hand, a quantitative analysis of the single-wavelength absorption amplitudes as a function of pump wavelength provides additional insight into the details of the relaxation dynamics in this system. Because the molecule ends up in the same fully thermalized excited state regardless of excitation energy, the long-time transient offsets ($\Delta t > 5$ ps, i.e., after all dynamics have ceased) at a given probe wavelength should yield identical levels of molecular absorption. This is usually not realized in practice due to variations in experimental conditions (e.g., pump power, pump/probe cross section, etc.) as the excitation wavelength is tuned. However, if we normalize data at a given probe wavelength to its long-time offset, we can correct for these experimental variations and obtain a quantitative comparison of the initial absorption amplitudes as a function of pump wavelength. As shown in Figure 8, this analysis reveals a systematic increase in the amplitude of the initial absorption on both the blue and red edges of the transient spectrum with increasing excitation energy. Since the data have been normalized to the long-time offsets this relative increase in ΔA at the wings corresponds to a broadening of the spectrum. This is wholly consistent with our model, which stipulates that higher-lying vibrational levels of the ^2E surface will show broader transient absorption spectra than lower-lying ones. The data in Figure 8 demonstrate that higher-energy pump photons result in the population of higher-lying vibrational levels within the ^2E state, leading to a greater degree of narrowing as the vibrational relaxation dynamics ensue.

This in turn gives us important information concerning vibrational dynamics on the $^4T_2$ surface. If vibrational relaxation

within this initially populated electronic state were occurring significantly faster than the $^4T_2 \rightarrow {}^2E$ conversion, a pump wavelength-dependent broadening of the excited-state absorption spectrum would not be observed. The surface crossing would always be proceeding from the lowest-lying vibrational level of the $^4T_2$, and our analysis would yield a constant value of c_1/a_0 versus pump energy. The fact that the initial absorption amplitude does vary systematically with excitation energy implies that the $^4T_2 \rightarrow {}^2E$ conversion is at the very least kinetically competitive with vibrational relaxation within the $^4T_2$ state.

Charge-Transfer Excitation. In addition to studying dynamics associated with ligand-field states, we also explored excitation into the charge-transfer manifold of the molecule. The vast majority of ultrafast work on transition metal complexes involves excitation to charge-transfer states. In both this and ongoing research, we hope to identify any systematic differences between ligand-field and charge-transfer dynamics. Excitation into the lowest-lying charge-transfer state of $Cr(acac)_3$ introduces roughly three times the amount of excess excitation energy when compared to ligand-field excitation. We wanted to address the question of whether the nonradiative coupling between the charge-transfer manifold and the ^2E surface differs appreciably from that of the $^4T_2$ ligand-field surface.

The long-time (nanosecond and slower) spectroscopy of the molecule is unaffected; as is the case with the majority of Cr^{III} complexes, the longest-lived excited state is the ^2E regardless of excitation energy. Analysis of the ultrafast data runs entirely in parallel with the results presented above. All dynamics are again complete within several picoseconds, resulting in an identical full spectrum at $\Delta t > 5$ ps. For times when 1 ps $< \Delta t < 5$ ps, the data are again dominated by narrowing of the excited-state absorption band without a discernible shift. The degree of narrowing is also consistent with the above discussion, as shown by the highest-energy point in Figure 8. The single-wavelength data, however, reveal an additional decay component at very early times. Figure 9 displays data for three different probe wavelengths following $^4A_2 \rightarrow {}^4$LMCT excitation at 335 nm. At probe wavelengths from 450 to 510 nm, a non-instrument-limited rise is observed, followed by decays quantitatively similar to the monoexponential kinetics observed under ligand-field excitation. As the probe wavelength is tuned toward the red, the amplitude of the fast component systematically decreases until it vanishes altogether near $\lambda_{probe} = 550$ nm; at this wavelength the dynamics are monoexponential. At probe wavelengths longer than 550 nm, the early-time component reappears with the same time constant, systematically increasing in amplitude with increasing λ_{probe}. In this region, however, the signal manifests itself as a decay rather than a rise. Fitting these latter data via iterative reconvolution with the instrument response function yielded a time constant of 50 ± 20 fs for this fast component.[65]

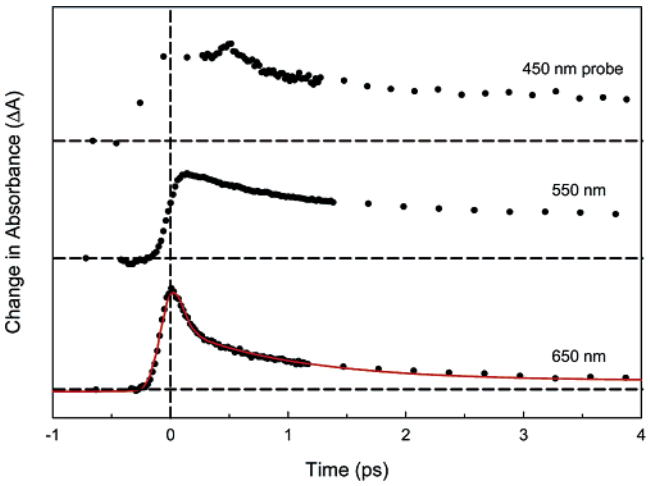

Figure 9. Time-resolved absorption data for $Cr(acac)_3$ following excitation at 335 nm at three probe wavelengths. The data at 650 nm were fit with iterative reconvolution of an instrument response function (Gaussian, 100 fs fwhm) with a biexponential decay function, yielding time constants of $\tau_1 = 50 \pm 20$ fs and $\tau_2 = 1.2 \pm 0.2$ ps.

The data just described can be explained under either of the following two scenarios. First, we could be seeing evidence of a dynamic shift of a single differential absorption feature to higher energy (i.e., a blue shift). This bears a strong analogy to the dynamic Stokes shifts often observed in ultrafast fluoresence spectroscopy.[66] In the present case, probe wavelengths to the red of λ_{max} will exhibit a loss in amplitude as the spectrum shifts to higher energy. Conversely, data sampling kinetics above the absorbance maximum (i.e., $\lambda_{probe} < \lambda_{max}$) will show a rising feature as the spectrum moves into the probe window. The feature will disappear entirely in probe regions where the slope of the absorbance feature is essentially zero over the range of wavelengths encompassing the blue shift. This can be realized for a very broad feature undergoing a relatively small change in λ_{max}.

A second possibility is the more classic case of two kinetically coupled species giving rise to two partially overlapping absorption spectra. In our case, the initial spectrum would correspond to the one furthest to the red. As this species decays, it gives rise to a new absorption at higher energy. Probe wavelengths to the red therefore sample the decay of the first component, whereas shorter wavelengths will record the formation of the second. If the spectra overlap, their intersection corresponds to an isosbestic where the differential absorption signal will remain invariant (i.e., no fast component will be observed).

The best way to distinguish between the two possibilities would be to examine full spectra as a function of time. Unfortunately, the combination of our time resolution, the small changes in amplitude associated with this early-time component, and the lower signal-to-noise ratio of our photodiode array relative to the single-wavelength measurements render us unable to extract a full spectrum profile of the short-lived transient. However, the relative simplicity of this compound does limit the number of possibilities we need to consider for the origin of this ~50-fs process, namely vibrational dynamics (spectral shift model) or conversion of the LMCT state to the ligand-field manifold (two-state model). There is inferential precedent for both of these assignments in the literature. Kovalenko and co-workers have studied the excited-state dynamics of stilbene and two aniline derivatives in a variety of solvents.[67] They report monophasic kinetics for vibrational cooling when solute−solvent

(65) At $\lambda_{probe} < 500$ nm, solvent-only signals around $\Delta t = 0$ (cf. 46) rendered us unable to precisely quantify the rise time.

(66) Stratt, R. M.; Maroncelli, M. *J. Phys. Chem.* **1996**, *100*, 12981−12996.
(67) Kovalenko, S. A.; Schanz, R.; Hennig, H.; Ernsting, N. P. *J. Chem. Phys.* **2001**, *115*, 3256−3273.

coupling is weak and an additional fast component that arises when stronger interactions (e.g., hydrogen bonds) are present. This latter process was ascribed to energy transfer to the solvent. An analogy may be drawn wherein excitation to a charge-transfer state in $Cr(acac)_3$ results in a larger degree of solute−solvent coupling than excitation to a ligand-field state which should be better insulated from solvent molecules. The second possibility, a conversion from the charge-transfer to ligand-field manifold, is reminiscent of dynamics we have documented following MLCT excitation of low-spin Fe^{II} polypyridyl complexes.[33,68] Initial formation of a ^{1}MLCT state in these systems is followed by a ~100-fs relaxation to excited ligand-field states, ultimately leading to formation of the lowest-energy excited state of the compound in <1 ps.

With the data we have available, we cannot definitively rule out either of these assignments.[69] It seems unlikely to us that vibrational energy transfer to the solvent would result in a large shift in the absorption spectrum of the excited state. In addition, preliminary measurements in CH_2Cl_2 solution did not reveal a significant change in the fast component as might be expected if the solvent were intimately involved in the relaxation mechanism. The parallels that are typically drawn between the chemistry of d^3 and low-spin d^6 metal complexes, though not directly transferable to excited-state dynamics, nevertheless make the ^{4}LMCT → LF assignment an attractive option to consider. The rate of an electronic surface crossing event is determined by the strength of nonradiative coupling between vibrational levels of the electronic states involved. This coupling is inversely proportional to the energy gap between two given vibrational states and directly proportional to the Franck−Condon overlap between them. Referring again to Figure 7, we may qualitatively anticipate that the relative energies of the two potential surfaces, in combination with significant horizontal displacement, serve to enhance the nonradiative coupling between the $^4T_2$ and ^{2}E states and result in the sub-100-fs time constant for this conversion. This in turn suggests that the rate of ^{4}LMCT → LF conversion (presumably the ^{2}E state) will be slower, given the larger energy gap and smaller nuclear displacement associated with these two states. We therefore tentatively assign the ~50-fs process in Figure 9 to the ^{4}LMCT → ^{2}E relaxation. Efforts to examine this process in more detail with improved time resolution are currently underway.

Concluding Comments

The ultrafast dynamics of $Cr(acac)_3$ have been studied with the goal of defining the time scale and mechanism of excited-state formation in this prototypical Cr^{III} complex. Following ligand-field excitation, the $^4T_2 \rightarrow {}^2$E conversion is found to occur within our experimental time resolution of 100 fs. A narrowing of the differential absorption spectrum is assigned to vibrational relaxation on the ^{2}E surface with a time constant of 1.1 ± 0.1 ps. Under charge-transfer excitation, an additional process is observed with a time constant of ~50 fs. This early-time component is tentatively assigned to the decay of the initially populated ^{4}LMCT state of the complex to the ^{2}E state. The resulting picture of excited-state evolution in $Cr(acac)_3$ is summarized in Figure 10.

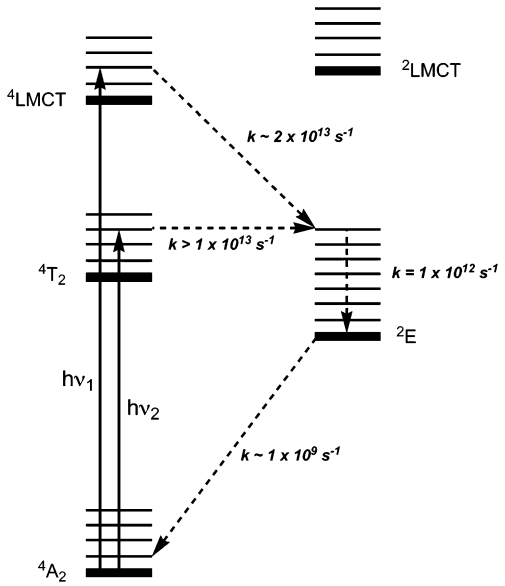

Figure 10. Simplified Jablonski diagram for $Cr(acac)_3$. The rates shown derive from the time constants obtained from the ultrafast time-resolved absorption studies discussed in this article.

The electronic structures of transition metal complexes routinely exhibit several important differences when compared to the organic molecules that form the basis for most models of ultrafast relaxation. A larger number of vibrational modes, particularly modes of low frequency, may serve to enhance rates of vibrational relaxation. Relatively large nuclear equilibrium displacements of low-lying excited states, particularly those of ligand-field states, may also greatly enhance electronic surface crossings, even to the point of exceeding vibrational relaxation processes within a given electronic state. The data we have presented for $Cr(acac)_3$ represent a case study in this regard.

The influence of equilibrium nuclear displacement on electronic surface crossings has recently been examined and even quantified for an organic system.[70] The observed rapid surface crossings were attributed to an increase in nuclear equilibrium displacement for certain excited states. A similar argument was suggested to explain subpicosecond internal conversion in the radiationless decay of DNA nucleosides.[71] Displacements considered uncommonly large for organic molecules are much more commonplace in systems containing transition metals. These factors, combined with an increased density of states, may prove to be a unifying theme when comparing the ultrafast dynamics of transition metal complexes to those of smaller molecules. Systematic study of relaxation dynamics as a function of energy gap as well as equilibrium nuclear displacement is a focus of ongoing research in our group.

Acknowledgment. This work was generously supported by the National Science Foundation (Grant No. CHE-0213505). We would also like to thank Dr. Sherri McFarland and Dr. Karen Cheng of Dalhousie University for assistance in writing the deconvolution software.

JA042153I

(68) Smeigh, A.; McCusker, J. K. Manuscript in preparation.
(69) Due to irreversible redox chemistry, we were unable to acquire spectroelectrochemical data on $Cr(acac)_3$, which would have aided in estimating where absorptions from the ^{4}LMCT state might occur.
(70) Fidder, H.; Rini, M.; Nibbering, E. T. J. *J. Am. Chem. Soc.* **2004**, *126*, 3789−3794.
(71) Pecourt, J. L.; Peon, J.; Kohler, B. *J. Am. Chem. Soc.* **2001**, *123*, 10370−10378.